Journal of Materials Chemistry A

Na ion Dynamics in P2-Nax[Ni1/3Ti2/3]O2: A Combination of Quasi-Elastic Neutron Scattering and First-Principles Molecular Dynamics Study

Journal:	*Journal of Materials Chemistry A*
Manuscript ID	TA-ART-08-2020-008400.R1
Article Type:	Paper
Date Submitted by the Author:	29-Oct-2020
Complete List of Authors:	Chen, Qian; Michigan State University, Chemical Engineering and Materials Science Jalarvo, Niina; Oak Ridge Na, Chemical and Engineering Materials Divisio Lai, Wei; Michigan State University, Chemical Engineering and Materials Science

SCHOLARONE™
Manuscripts

Na ion Dynamics in P2-$Na_x[Ni_{1/3}Ti_{2/3}]O_2$: A Combination of Quasi-Elastic Neutron Scattering and First-Principles Molecular Dynamics Study

Qian Chen[1], Niina H. Jalarvo[2], and Wei Lai[1]

[1] Department of Chemical Engineering and Materials Science, Michigan State University, East Lansing, MI 48824, USA

[2] Neutron Scattering Division, Oak Ridge National Laboratory, Oak Ridge, Tennessee 37831-6475, United States

ABSTRACT

In this work, the P2-type layered material $Na_{2/3}[Ni_{1/3}Ti_{2/3}]O_2$ was studied as a promising bi-functional electrode material for sodium-ion batteries. To assess the electrochemical performance of this material, we investigated the diffusion mechanism as well as ionic and electronic conductivity with a combination of experimental and computational techniques. The quasi-elastic neutron scattering (QENS) experiments and first-principles molecular dynamics (FPMD) simulations were performed to identify the diffusion mechanism. The QENS data showed that Na ion diffusion can be well described by the Singwi-Sjölander jump diffusion model, where the obtained mean jump length matched the distances between the neighboring edge-share and face-share Na sites. FPMD predicted diffusivity values similar to those from QENS. The computed composition dependence of ionic and electronic conductivity of $Na_x[Ni_{1/3}Ti_{2/3}]O_2$ suggested that electronic conductivity changes significantly when x deviates from 2/3 as the redox couple of Ni and Ti being activated, while the change of ionic conductivity with x is relatively small.

Introduction

The increasing demands of integrating intermittent renewable energy sources into the electric grid bring in new challenges in developing large-scale electrochemical energy storage systems at low cost[1,2]. The sodium-ion batteries are considered as a promising alternative to the currently dominant lithium-ion batteries for grid-scale energy storage, because of the low cost and huge natural abundance of sodium resources[3,4]. Tremendous research efforts have been devoted to developing sodium-ion batteries, especially in the search of electrode materials for better performance[5-7]. Among the candidates, layered sodium transition metal (TM) oxides Na_xTMO_2 oxides have attracted intensive attention due to their high capacities[8,9], such as $Na_{2/3}[Ni_{1/3}Mn_{2/3}]O_2$[10], $Na_{2/3}[Mg_{0.28}Mn_{0.72}]O_2$[11], and $Na_{2/3}[Fe_{1/2}Mn_{1/2}]O_2$[12].

Among the layered oxide materials, we are particularly interested in $Na_{2/3}[Ni_{1/3}Ti_{2/3}]O_2$ as it showed good electrochemical performance as both negative (due to Ti) and positive (due to Ni) electrodes[13]. Compared to most electrode materials that can only be used in non-symmetric cells, such bi-functional electrode materials could lead to additional benefits of reduced cost and simpler fabrication[14,15].

Figure 1a shows the crystal structure of $Na_{2/3}[Ni_{1/3}Ti_{2/3}]O_2$. The structure is classified as P2-type by Delmas et al.[16] with 2 layers of TMO_6 octahedra in the unit cell and Na ions residing in two prismatic sites, the edge-share sites (Na_e) sharing edges and face-share sites (Na_f) sharing faces with the TMO_6 octahedra. The nearest-neighbor edge and face-share Na sites form a 2D honeycomb lattice where the Na ions could diffuse (Figure 1b), as found in $Na_{2/3}[Ni_{1/3}Ti_{2/3}]O_2$ in our previous study[17] and in other P2-type materials[18].

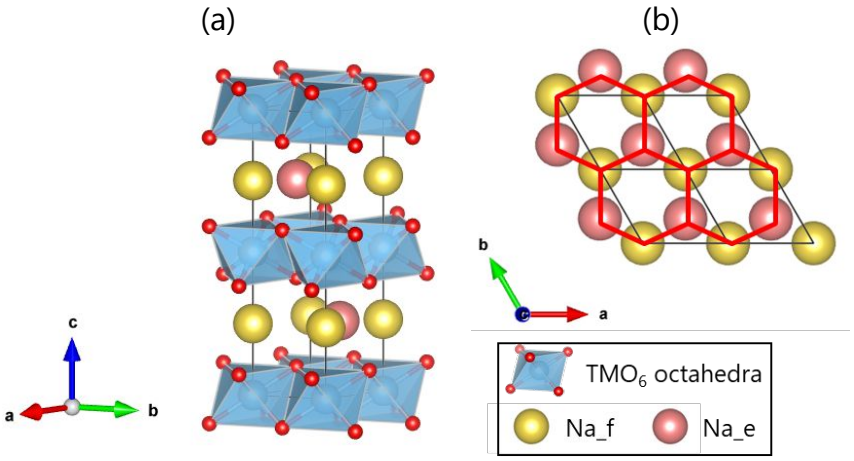

Figure 1: (a) The structure of P2-$Na_{2/3}[Ni_{1/3}Ti_{2/3}]O_2$ viewed along the *ab* plane (b) The $2a \times 2b$ Na layer viewed along the *c* axis. The red lines show the honeycomb-shaped Na diffusion pathway.

While important electrode properties such as ionic and electronic conductivity have been measured for this material with macroscopic methods in previous studies[19-21], the atomic level investigation is needed to reveal the underlying mechanism of transport processes. In our previous study[17], the MD simulation based on polarizable interatomic potential (IP) model was applied to calculate the diffusivity and ionic conductivity of P2-

$Na_{2/3}[Ni_{1/3}Ti_{2/3}]O_2$. However, as the IP model relies on parametric forces, it tends to neglect the underlying electronic origin of the interactions. Higher accuracy can be achieved by using first-principle calculations such as density-functional theory (DFT) to describe the interatomic interactions for MD, which captures the changes in chemical bonding during dynamic events. In this study, we employed DFT based MD simulations which could describe more accurately the ion and electron transport in P2-$Na_{2/3}[Ni_{1/3}Ti_{2/3}]O_2$. In addition, we, for the first time, reported quasi-elastic neutron scattering (QENS)[22] experiments to measure diffusive motions of P2-$Na_{2/3}[Ni_{1/3}Ti_{2/3}]O_2$ that can provide both temporal and microscopic spatial information on atomic dynamics, compared with nuclear magnetic resonance (NMR) experiments that only yield temporal information. As high diffusivity, high ionic and electronic conductivities are desired for electrodes, we further calculated these properties for Na-deficient phase $Na_{5/9}[Ni_{1/3}Ti_{2/3}]O_2$ and Na-rich phase $Na_{7/9}[Ni_{1/3}Ti_{2/3}]O_2$ to examine the electrochemical performance of the material upon cycling as either positive and negative electrodes.

Methods

Experimental methods

$Na_{2/3}[Ni_{1/3}Ti_{2/3}]O_2$ powders were synthesized by solid-state reactions with stoichiometric amounts of Na_2CO_3 (≥99.5%,), NiO (99%), and TiO_2 (≥99%) precursor powders, all from Sigma-Aldrich. The mixed precursor powders were dry-milled and then fired at 900 ^oC for

12 hours. The obtained $Na_{2/3}[Ni_{1/3}Ti_{2/3}]O_2$ powders were heated to 200 ^oC for 10 hours and then stored in an argon atmosphere to limit the exposure to moisture.

QENS experiments were conducted using the time-of-flight backscattering spectrometer (BASIS)[23] at the Oak Ridge National Laboratory (ORNL). The measurements were performed from 450 to 700 K to study the Na ion dynamics and at 30 K for the instrument resolution function. The data were normalized by the Vanadium measurement and reduced in the Mantid package[24], with the energy transfer (*E*) range of ±100 μeV (0.4 μeV binning) and momentum transfer (*Q*) range of 0.3 to 1.9 $Å^{-1}$ (0.2 $Å^{-1}$ binning). The QENS spectra at each *Q*, with a convolution of the resolution function, were fitted with a combination of one delta function (for the elastic peak), a Lorentzian peak (for the quasi-elastic features), and a flat background using the DAVE package[25]. The broadening of the QENS spectra resulted from the diffusive motions in the sample was quantified by the half-width-half-maximum (HWHM or Γ) of the Lorentzian peak. The diffusive properties were calculated based on the *Q*-dependence of the broadening. For large distances (small *Q*), the Fickian diffusivity *D* was extracted from the linear relationship between *Γ* and Q^2 as $\Gamma=DQ^2$. At smaller distances, the *Q*-dependence of *Γ* was described by the Singwi-Sjolander (SS) jump model[26], where the jumps are characterized by the residence time τ and mean jump distance *r* in the SS model as the following:

$$\Gamma = \frac{1}{\tau}\left(\frac{Q^2 < r^2 > /6}{1 + Q^2 < r^2 > /6}\right)$$

Simulation details

The DFT calculations were performed using the Vienna Ab initio Simulation Package (VASP)[27] within the projector augmented-wave (PAW) approach[28] using the dispersion-corrected Perdew-Burke-Ernzerhof with Becke-Jonson damping (PBE-D3BJ) functional[29,30]. The non-spin-polarized calculations were performed with a plane-wave energy cut-off of 450 eV and a single Γ point. The Hubbard U correction was applied to Ni considering the on-site Coulomb interactions between 3d electrons. The U value for Ni was selected to be 6.2 eV[31], which was well tested for this system in our previous study[17]. The starting structure for pristine $Na_{2/3}[Ni_{1/3}Ti_{2/3}]O_2$ was a 3 × 3 × 1 supercell containing 66 atoms. The configurations for $Na_{7/9}[Ni_{1/3}Ti_{2/3}]O_2$ and $Na_{5/9}[Ni_{1/3}Ti_{2/3}]O_2$ as the Na-rich and Na-deficient phases were generated by randomly adding and removing Na atoms from the pristine phase while maintaining the same number of Na atoms in each layer. DFT-based MD simulations with the NVT ensemble were performed at 900, 1000, and 1100 K with an equilibrium time of 3 ps and production run time ranging from 20 ps to 100 ps. For all compositions, the lattice parameters were determined based on an NPT ensemble run of 3ps. The lattice parameters were reported in our previous study[17]. Convergence tests for the trajectory time and correlation time were performed before we extracted the diffusivity to make sure we have long enough trajectory and correlation time. The time step was 1 fs for all temperatures. For the electronic conductivity calculations, 50 input structures were randomly selected from the MD trajectory for each composition. The DFT

electronic structure calculations were conducted for each configuration with a cut-off energy of 450 eV and a Gamma-centered k-mesh of 4×4×3. The electrical conductivities were calculated using maximally localized Wannier functions as basis functions with the BoltzWann module[3] in the Wannier90 package[2] based on the semiclassical Boltzmann transport equations. The relaxation time was approximated as a constant value of 10 fs.

Results and Discussion

Na ion diffusion in $Na_{2/3}[Ni_{1/3}Ti_{2/3}]O_2$

In QENS experiments, the quasi-elastic broadening of spectra was the direct evidence of diffusive motions, as shown in the measured QENS spectra S(Q, E) for Q=0.3 $Å^{-1}$, i.e. Figure 2. The inset plot in Figure 2 shows the increased QENS broadening with increasing temperature, suggesting enhanced diffusion at higher temperatures.

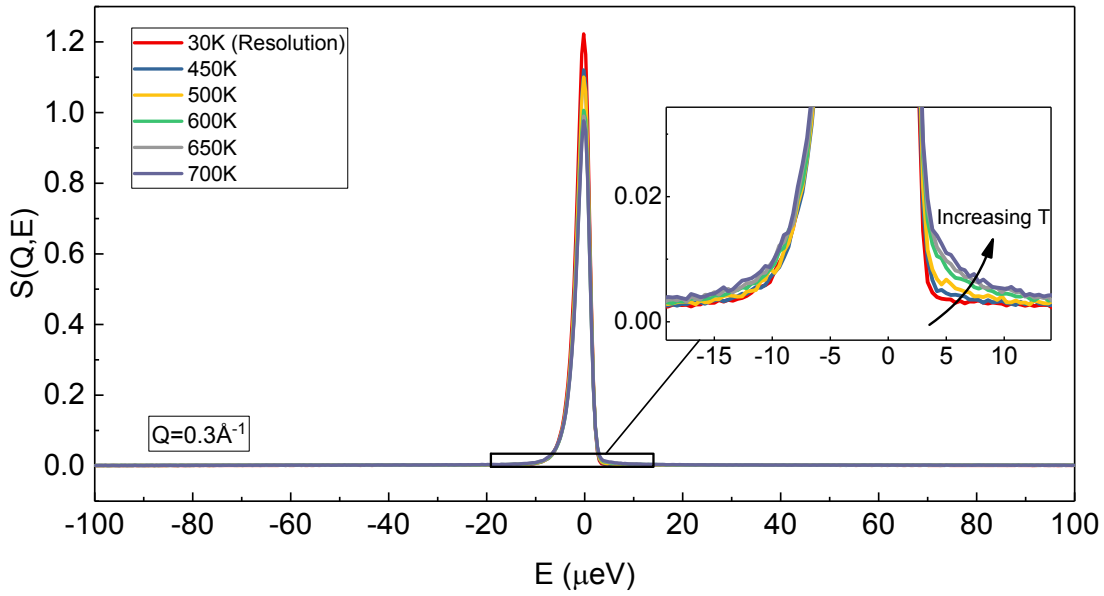

Figure 2: Experimental QENS spectra S(Q,E) for various temperatures at Q=0.3 $Å^{-1}$.

The quantitative analysis of spectra was conducted to further understand the Na diffusion behaviors in the sample. The measured QENS data at each temperature and each *Q*, was fitted with a combination of a flat background, one delta function for the elastic peak and a Lorentzian peak for the quasi-elastic features, convoluted with the resolution function. An example for 700 K and Q=0.3 $Å^{-1}$ shows the fit and residuals in Figure 3(a). The Q-dependence of half-width-half-maximum (HWHM or Γ) of the Lorentzian peak characterizes the diffusive motions of Na. Figure 3(b) shows an example of Γ against Q at 700 K.

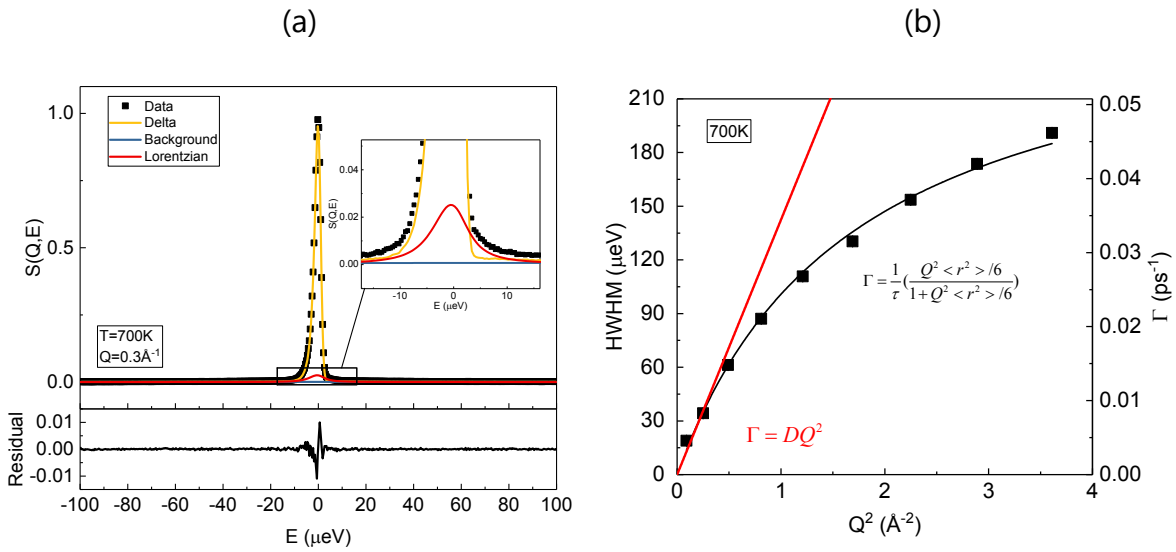

Figure 3: (a) Fit of the QENS spectra at 700 K and Q=0.3 $Å^{-1}$. (b) The HWHM of the Lorentzian function at 700 K as a function of Q^2, fitted to the Fickian model at small Q (red line) and the SS model (black line).

In the low-Q region, a linear relationship between Γ and Q^2 indicates continuous translational diffusion of Na ions following Fick's law at large distances. The Fick's law describes the continuous diffusion, which is only observed at long distances (low Q).

The Fickian diffusivity D was calculated according to $\Gamma(Q) = DQ^2$ in Q≤0.5 Å^{-1} range, as the slope of the red line in Figure 3(b). The Fickian diffusivity values extracted from the QENS spectra at different temperatures are plotted in Figure 4 (blue filled circles). The Na self-diffusivity in the temperature range of 450 to 700 K is on the order of 10^{-6} cm^2/s, which falls in the same range with the similar layered compound $Na_{0.8}CoO_2$ from a QENS study[32]. Based on the Arrhenius fit for the temperature dependence of Na self-diffusivity, we obtained an activation energy of 0.15 eV and a diffusivity of ~10^{-7} cm^2/s at room temperature. The low activation energy barrier of this material is comparable to some P2-type compounds including $Na_{2/3}[Ni_{1/3}Mn_{1/3}Ti_{1/3}]O_2$ (0.17 eV from FPMD[33]), $Na_{0.8}CoO_2$ (0.17eV at ~350K from QENS[32]), and $Na_x[Ni_{2/3}Mn_{2/3}]O_2$ with 1/3<x<2/3 (0.17eV from the Nudged Elastic Band (NEB) method[34]). It is lower than some other P2 compounds such as $Na_{0.6}[Cr_{0.6}Ti_{0.4}]O_2$ (0.35 eV from FPMD[35]), $Na_{5/6}Li_{1/12}Ni_{1/4}Mn_{2/3}O_2$ (0.28 eV from FPMD[36]).

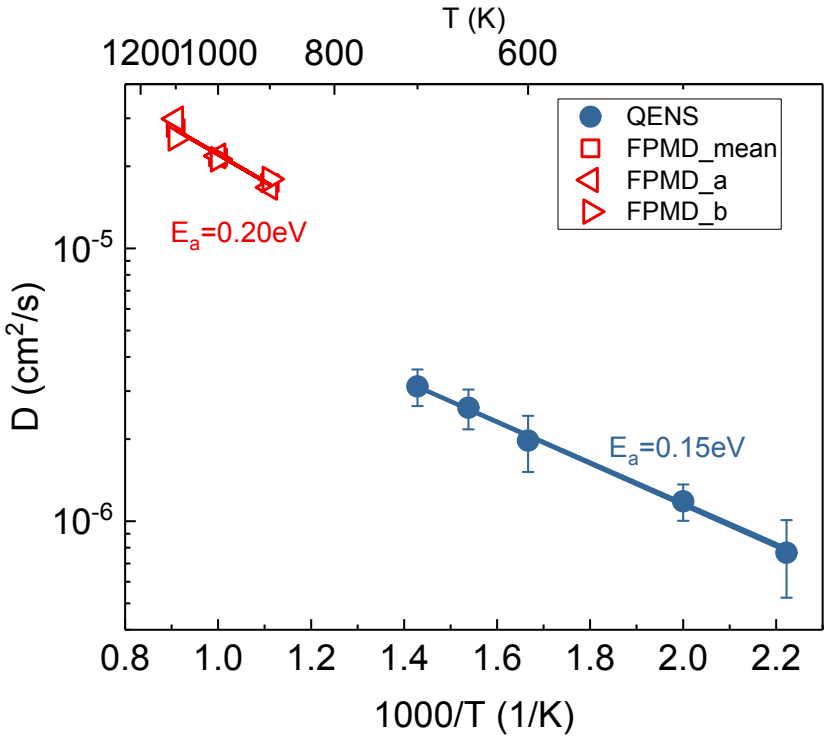

Figure 4: The Fickian self-diffusivity of Na obtained from QENS (blue filled circles) and FPMD (red triangles for D along [100] and [010], respectively, and, red squares for mean diffusivity along the xy plane)

At large Q (small distance), the deviation from the linear relationship between Γ and Q^2 with Γ approaching a plateau suggests localized jump behavior. The Singwi-Sjolander (SS) jump model[26] was used to describe the local dynamics of Na ions (black line in Figure 3(b)), where the average residence time τ and mean jump length r were obtained from the Q-dependence of Γ based on :

$$\Gamma(Q) = \frac{1}{\tau}\left(\frac{Q^2 < r^2 > /6}{1 + Q^2 < r^2 > /6}\right)$$

The mean jump length and residence time, rather than diffusion coefficients, were used to characterize the localized jumps described by the SS model. The mean jump length

and residence time obtained from the SS model with the temperature dependence are plotted in Figure 5. The jump lengths are between 1 and 2 Å which fit into the dimension of the honeycomb sublattice in the Na layer, as the distance from an edge-share site to a nearest-neighbor face-share site and vice versa is around 1.7 Å (the side length of red hexagons shown in Figure 1b). This confirms that Na primarily migrates between edge-share and face-share sites within the 2D diffusion pathway. The average jump length of Na increases with temperature, while the residence time decreases with temperature as more frequent and longer jumps can be activated by higher thermal energy.

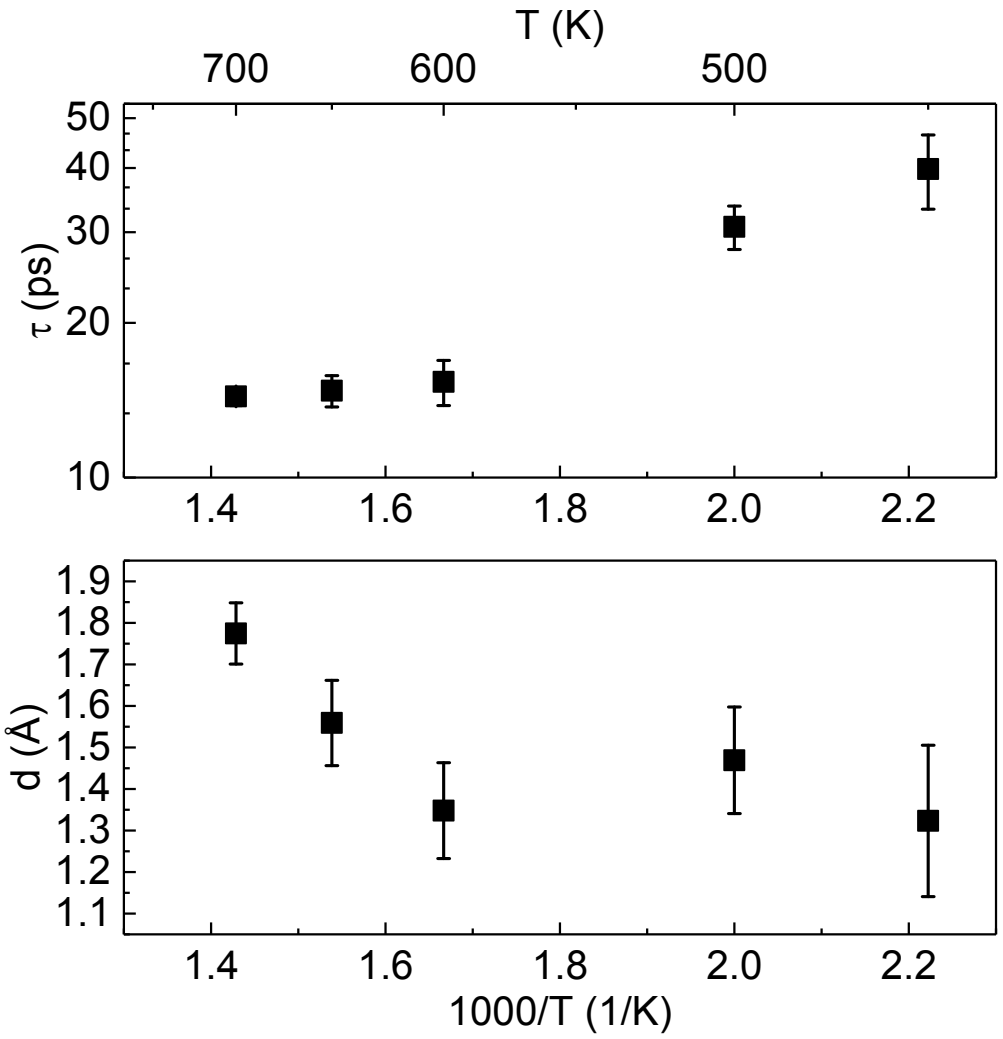

Figure 5: (a) The residence time and (b) mean jump length obtained from QENS based on Singwi-Sjolander jump model.

In addition to QENS experiments, the first-principles MD simulations were conducted to further understand the diffusion mechanism. The FPMD trajectory recording the positions of all Na ions provided the direct visualization of Na motion. We plotted the Na density maps from the MD trajectories as shown in Figure 6. Na density maps showed traces along the 2D honeycomb diffusion pathway in the Na layer, consistent with the jump length obtained from the QENS measurement.

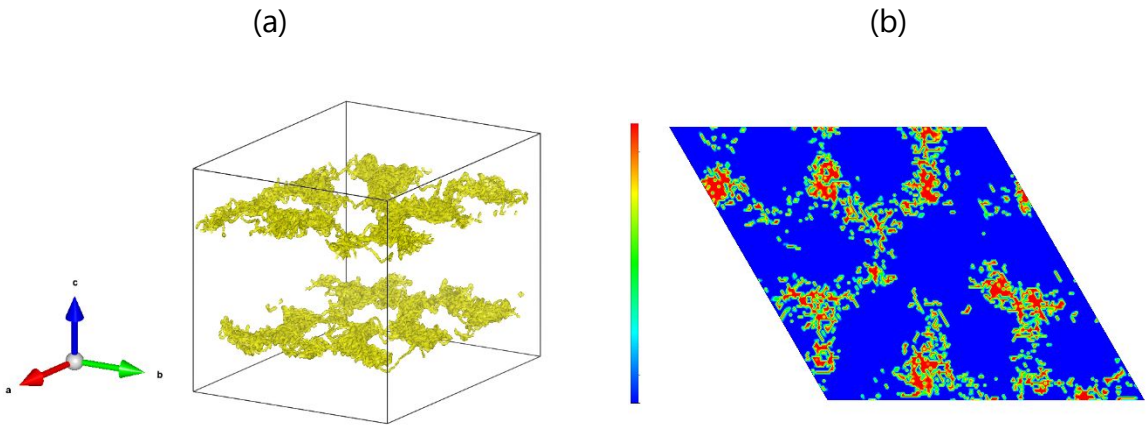

Figure 6: The nuclear density map of Na from 20 ps MD simulation trajectory at 1100 K. (a) 3D view with an isosurface level of 0.2 Å^{-3}, (b) 2D slice on the (001) lattice plane with an isosurface level of 0~0.5 Å^{-3}.

From the simulation, the Fickian self-diffusion coefficient along direction X was calculated by the Green-Kubo integration of velocity autocorrelation function:

$$D_{\alpha}^{X} = \frac{1}{N_{\alpha}} \sum_{i=1}^{N_{\alpha}} \int_{0}^{\infty} \langle v_i^X(t) \cdot v_i^X(0) \rangle dt$$

where N_α stands for the total number of atom α and v_i^X the X-direction component of velocity for the i^{th} atom. The Green-Kubo integral reached a plateau within a short correlation time. For D_{α}^{X} along the c axis, the integral plateaued around 0, suggesting no cross-plane diffusion, consistent with what we observed from the Na density maps. The diffusion coefficients along *a* and *b* axis were obtained by averaging over a correlation time period in the plateau region (we selected 2-3 ps in this work).

The Fickian self-diffusivity along *a* and *b* axis as well as the averaged value over two directions in the temperature range 900 to 1100 K are plotted in Figure 4. The diffusivity extracted from the MD simulation is about two times higher than those from the QENS

experiment when extrapolating to the same temperature. The activation energy obtained from the Arrhenius equation for in-plane Na diffusion from 900 to 1100 K is 0.20 eV which is slightly higher than QENS results (0.15 eV).

While the FPMD simulation provides comparable results with the QENS experiment for the pristine material of sodium content x=2/3, to assess the Na diffusivity change during cycling, we further calculated the diffusivity with the same approach for the other two compositions of x=5/9 and 7/9. Figure 7 shows the calculated Na in-plane Fickian diffusivity for the three compositions at 900 K. From x=2/3 to x=5/9, $Na_{5/9}[Ni_{1/3}Ti_{2/3}]O_2$ shows a comparable diffusivity to $Na_{2/3}[Ni_{1/3}Ti_{2/3}]O_2$ with only 3% of increase. This trend is consistent with the diffusivity measured in this x range for $Na_x[Ni_{1/3}Ti_{2/3}]O_2$[19] as well as in other P2-type compounds[33,34,37] using the Potentiostatic Intermittent Titration Technique (PITT) method. From x=2/3 to x=7/9, the insertion of Na ions into the pristine material leads to a significant drop of the diffusivity, which can be attributed to the limited number of vacant sites.

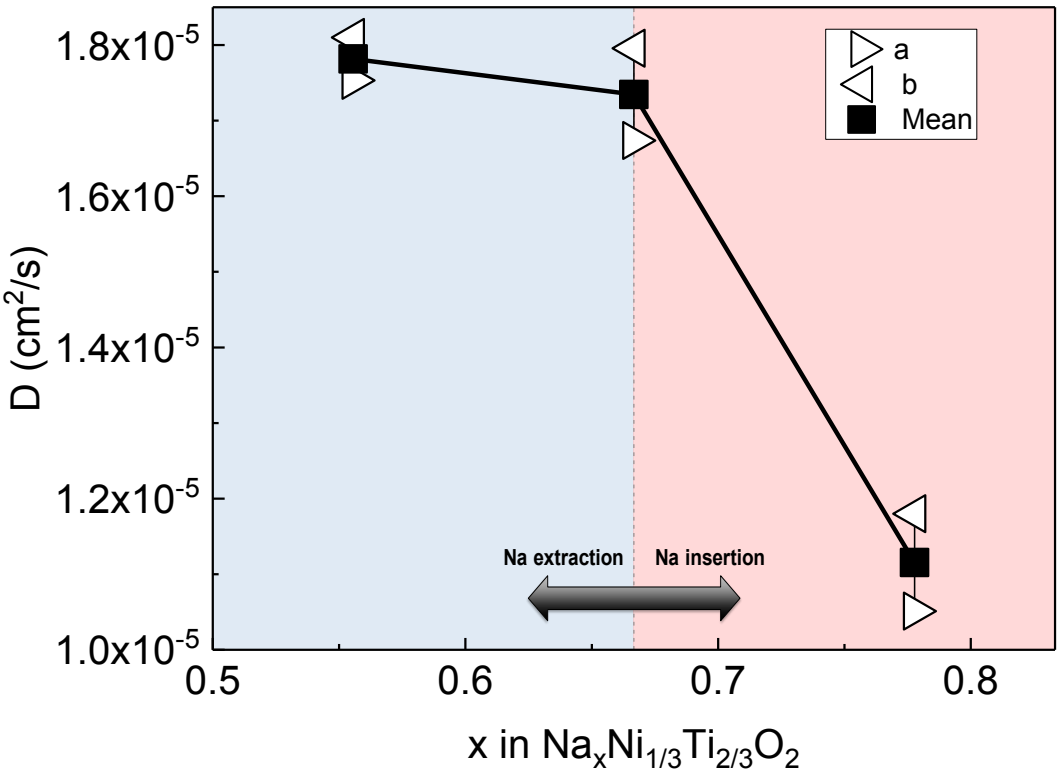

Figure 7: Calculated Fickian diffusivity from FPMD simulation at 900 K for different sodium content.

Ionic conductivity

As the sodium diffusivity predicted by our first-principles MD simulations showed good consistency with the experiments, the ionic conductivity was also assessed using the MD trajectories. The ionic conductivity was calculated based on the Green-Kubo relations:

$$\sigma = \frac{1}{k_B T V}\int_0^\infty \langle J^X(t) J^X(0)\rangle dt$$

where k_B is the Boltzmann constant, V the volume of the system, and T the temperature. The J^X represents the X-direction component of the charge current $\boldsymbol{J} = \sum_{i=1}^{N} q_i \boldsymbol{v}_i(t)$. The

charge carried by the i^{th} atom q_i was calculated using Density Derived Electrostatic and Chemical (DDEC6) charge analysis in our previous study[17]. Similar to diffusion, the integral of charge current correlation along *c* axis converged to a plateau around zero within 1 ps, suggesting a 2D ionic conduction within the layers. The ionic conductivities along *a* and *b* axis were calculated from the mean integral of charge current correlation over correlation time range from 2 to 3 ps. In-plane ionic conductivity at 900, 1000, and 1100 K were obtained by averaging the results along *a* and *b* axis as shown in Figure 8, along with computational results from our previous study based on the interatomic potential (IP) model[17] and experimental results from Shanmugam et al.[19], Shin et al. [20], and Smirnova et al.[21] Calculated in-plane ionic conductivities from the FPMD, if extrapolated to lower temperatures, are slightly higher than experimental results. The calculated activation energy was 0.27 eV, comparable to the experimental values, while our previous work with the IP model had a larger activation energy of 0.37 eV

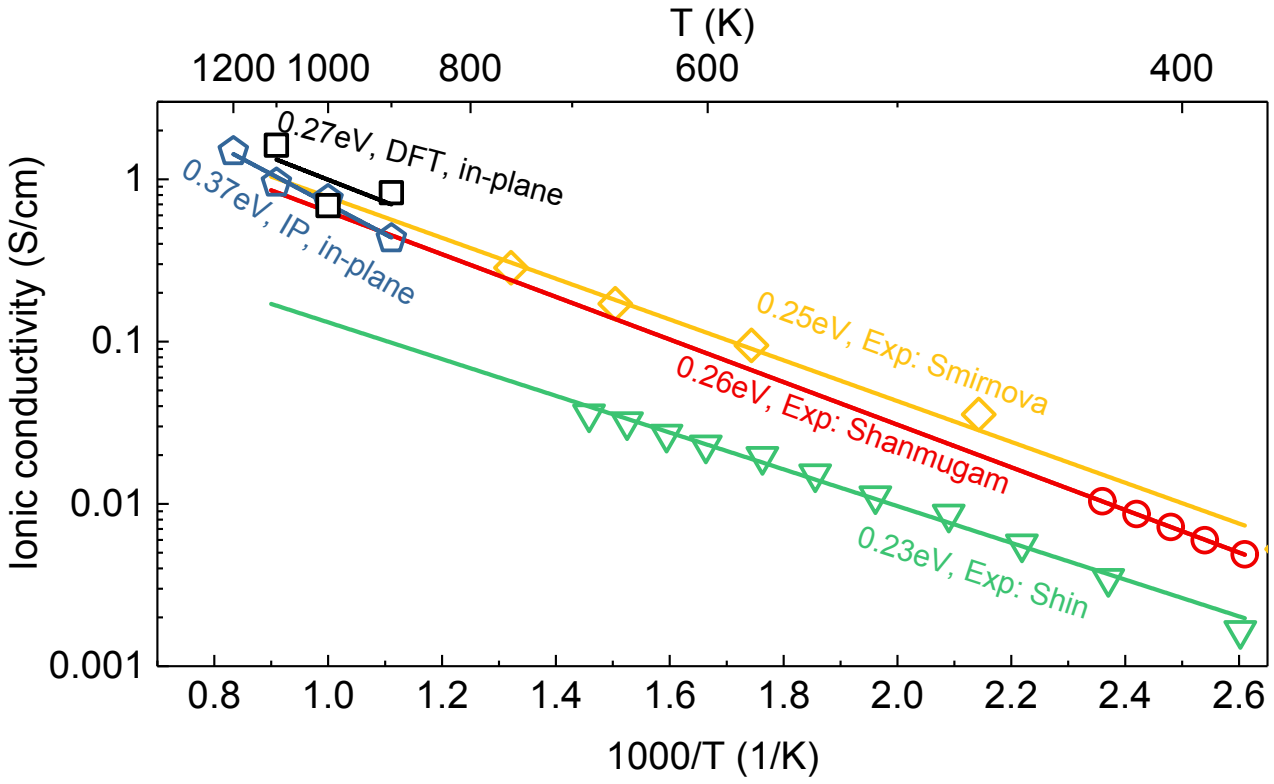

Figure 8: Calculated in-plane ionic conductivity of $Na_{2/3}Ni_{1/3}Ti_{2/3}]O_2$ compared with computational values from Chen et al.[17] and experimental data from Shanmugam et al.[19], Shin et al.[20], and Smirnova et al.[21]

The Na concentration-dependence of the ionic conductivity was examined by calculating the conductivity values at 900 K for the other two compositions $Na_{5/9}[Ni_{1/3}Ti_{2/3}]O_2$ and $Na_{7/9}[Ni_{1/3}Ti_{2/3}]O_2$. As shown in Figure 9, both Na-deficient phase $Na_{5/9}[Ni_{1/3}Ti_{2/3}]O_2$ and Na-rich phase $Na_{7/9}[Ni_{1/3}Ti_{2/3}]O_2$ showed higher ionic conductivity compared to the pristine phase. From x=2/3 to x=5/9, when Na atoms are extracted from the pristine $Na_{2/3}[Ni_{1/3}Ti_{2/3}]O_2$, the increase of ionic conductivity is likely to be related to increased vacancies. From x=2/3 to x=7/9, when the Na atoms are inserted to $Na_{2/3}[Ni_{1/3}Ti_{2/3}]O_2$, higher ionic conductivity can be achieved with more charge carriers.

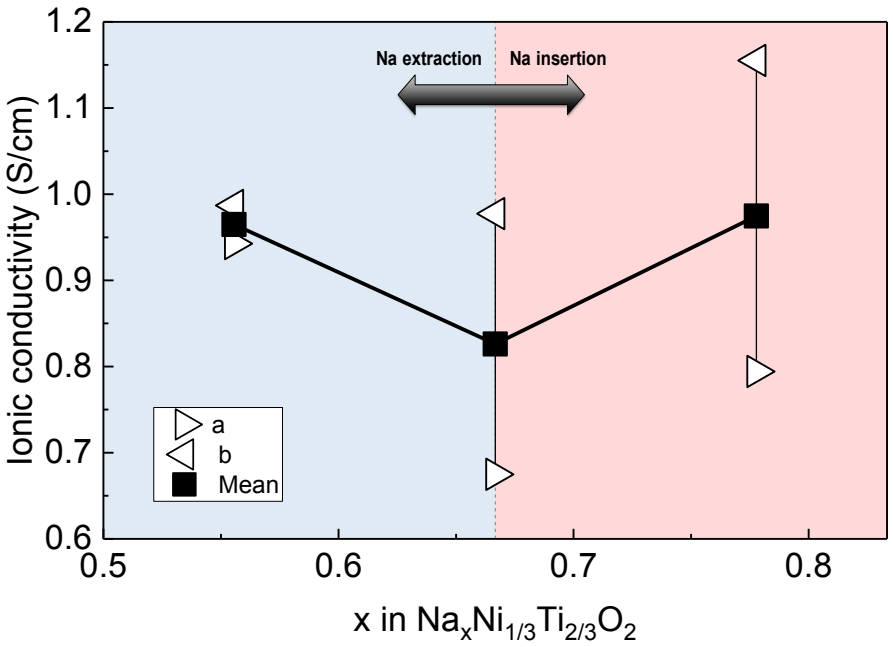

Figure 9: The calculated in-plane ionic conductivity from FPMD simulation at 900 K for different sodium content.

Electronic conductivity

The electronic conductivities of P2-$Na_x[Ni_{1/3}Ti_{2/3}]O_2$ at different x were also calculated. For each composition, calculations were carried out for 50 configurations randomly selected from the MD trajectory to account for the dynamics in the material. Despite the limitation of the DFT+U method in choosing the semi-empirical U values, the electronic structure calculations still provide valuable insights in the Na concentration dependence of the electronic conductivity of this material. Figure 10 shows the calculated electronic conductivity in three directions along the Cartesian *x*, *y*, and *z* for three different compositions. Each data point represents the value calculated from one individual structure, while the box gives the standard deviation of the data. The numbers in the plot label the average calculated electronic conductivities for all configurations of a composition.

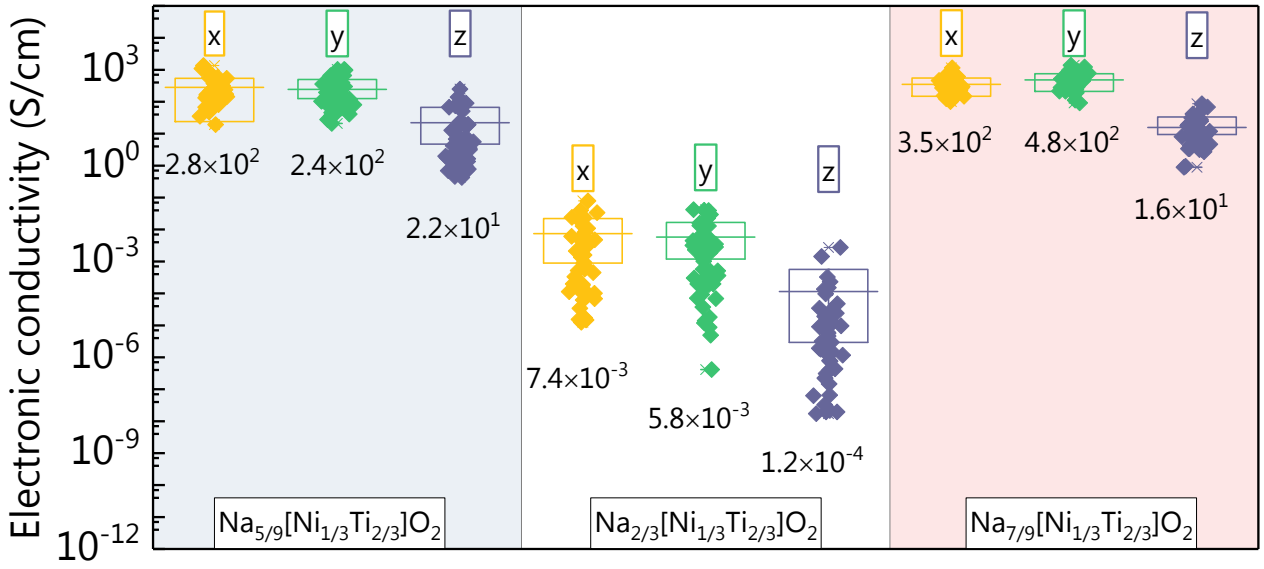

Figure 10: The electrical conductivity of $Na_x[Ni_{1/3}Ti_{2/3}]O_2$ at different x. The left, middle, and right panel represents results for $Na_{5/9}[Ni_{1/3}Ti_{2/3}]O_2$, $Na_{2/3}[Ni_{1/3}Ti_{2/3}]O_2$, $Na_{7/9}[Ni_{1/3}Ti_{2/3}]O_2$, respectively.

Yellow, green and purple points represent the calculated electrical conductivity along x, y and z direction, respectively.

It is clear that electronic conductivity is sensitive to atomic structure as its value varies significantly, by orders of magnitude, for different configurations. For all compositions, electronic conductivities observed along the Cartesian *x* and *y* directions are about one order's magnitude higher than that along the *z* (i.e. crystallographic *c*) direction, suggesting the mainly two-dimensional electron conduction. However, the electronic conductivity along the *z* direction (e.g. ~10 S/cm) of Na rich and deficient phases is not negligible, unlike the case of ionic conductivity. There is a significant increase (about 5 order's magnitude) in the electronic conductivity when sodium content is decreased or increased from the pristine phase by 16.7% (i.e. from x=2/3 to x=5/9 and from x=2/3 to x=7/9). This trend is consistent with our previous study with a single configuration calculation based on the Kubo-Greenwood approach[17]. This significant increase of electronic conductivity is not surprising as the pristine phase of $Na_{2/3}[Ni_{1/3}Ti_{2/3}]O_2$ contains nominally Ni^{2+} and Ti^{4+}, while decrease or increase of Na content will activate Ni^{2+}/Ni^{3+} or Ti^{4+}/Ti^{3+} redox couple, respectively.

Conclusions

In this work, the P2-type layered material $Na_x[Ni_{1/3}Ti_{2/3}]O_2$ was investigated with a combination of quasi-elastic neutron scattering and density-functional theory to study the Na ion diffusion mechanism and ionic and electronic conduction. Firstly, based on the Q-dependence of the quasi-elastic broadening in QENS measurement, the localized Na

ion diffusion behavior can be described by the Singwi-Sjölander jump model. The extracted average jump lengths are around 1.3~1.8 Å at 450~700 K, corresponding to the distance between the neighboring edge-share and face-share sites. This is also consistent with the diffusion mechanism revealed by the density maps from MD simulations: 2D local jumps occur between the edge-share and face-share Na sites. More frequent and longer jumps were observed at higher temperatures. For long-range diffusivity, Fick's model was applied to compare with the MD simulation results where $Q \rightarrow 0$. The QENS showed a Fickian diffusivity in the order of ~10^{-6} cm2/s from 450 to 700 K with E_a = 0.15 eV. The MD simulation gave an in-plane diffusivity of ~10^{-5} cm^2/s with E_a = 0.20 eV in the temperature range of 900 to 1100 K. The diffusion coefficients were calculated for different compositions with the Na concentration x in the range of 5/9 to 7/9. Faster diffusion was observed for compositions with less sodium, i.e., more vacancies. Secondly, the MD simulations showed in-plane ionic conductivity values ~ 1 S/cm at 900 to 1100 K with an activation energy of 0.27 eV, which is in good consistency with experimental measurements in previous studies. Both Na-deficient phase $Na_{5/9}[Ni_{1/3}Ti_{2/3}]O_2$ and Na-rich phase $Na_{7/9}[Ni_{1/3}Ti_{2/3}]O_2$ showed higher ionic conductivity compared to the pristine phase. Finally, for all the three compositions studied in this work (x=5/9, 2/3, and 7/9), the electronic conductivity in the *x* and *y* direction showed one order higher values compared to *z* direction. The pristine $Na_{2/3}[Ni_{1/3}Ti_{2/3}]O_2$ showed an electronic conductivity of ~10^{-3} S/cm, of which a significant increase can be achieved by either removing or inserting Na

ions. Removing or inserting 16.7% of the Na can lead to an increase in the electronic conductivity of 5 orders.

Acknowledgments

This work is financially supported by the CAREER grant from the Ceramics Program of National Science Foundation (DMR-1554315). The neutron experiments used resources at the Spallation Neutron Source, a DOE Office of Science User Facility operated by the Oak Ridge National Laboratory. We would like to thank the High Performance Computing Center and the Institute for Cyber-Enabled Research at Michigan State University for providing the computational resources.

References

(1) B. Dunn, H. Kamath, and J.-M. Tarascon "Electrical Energy Storage for the Grid: A Battery of Choices," *Science* **2011**, *334*, 928-935. http://dx.doi.org/10.1126/science.1212741

(2) D. Larcher and J. M. Tarascon "Towards greener and more sustainable batteries for electrical energy storage," *Nat Chem* **2015**, *7*, 19-29. http://dx.doi.org/10.1038/nchem.2085

(3) C. Vaalma, D. Buchholz, M. Weil, and S. Passerini "A cost and resource analysis of sodium-ion batteries," *Nat Rev Mater* **2018**, *3*.

(4) T. Liu, Y. Zhang, Z. Jiang, X. Zeng, J. Ji, Z. Li, X. Gao, M. Sun, Z. Lin, M. Ling, J. Zheng, and C. Liang "Exploring competitive features of stationary sodium ion batteries for electrochemical energy storage," *Energy & Environmental Science* **2019**, *12*, 1512-1533. http://dx.doi.org/10.1039/C8EE03727B

(5) N. Yabuuchi, K. Kubota, M. Dahbi, and S. Komaba "Research Development on Sodium-Ion Batteries," *Chem Rev* **2014**, *114*, 11636-11682. http://dx.doi.org/10.1021/cr500192f

(6) J. Deng, W.-B. Luo, S.-L. Chou, H.-K. Liu, and S.-X. Dou "Sodium-Ion Batteries: From Academic Research to Practical Commercialization," *Advanced Energy Materials* **2018**, *8*, 1701428. http://dx.doi.org/10.1002/aenm.201701428

(7) Y. Li, Y. Lu, C. Zhao, Y.-S. Hu, M.-M. Titirici, H. Li, X. Huang, and L. Chen "Recent advances of electrode materials for low-cost sodium-ion batteries towards practical application for grid energy storage," *Energy Storage Materials* **2017**, *7*, 130-151. http://dx.doi.org/10.1016/j.ensm.2017.01.002

(8) P.-F. Wang, Y. You, Y.-X. Yin, and Y.-G. Guo "Layered Oxide Cathodes for Sodium-Ion Batteries: Phase Transition, Air Stability, and Performance," *Advanced Energy Materials* **2018**, *8*, 1701912. http://dx.doi.org/10.1002/aenm.201701912

(9) K. Kubota, S. Kumakura, Y. Yoda, K. Kuroki, and S. Komaba "Electrochemistry and Solid-State Chemistry of NaMeO2 (Me = 3d Transition Metals)," *Advanced Energy Materials* **2018**, *8*, 1703415. http://dx.doi.org/10.1002/aenm.201703415

(10) Z. Lu and J. R. Dahn "In Situ X-Ray Diffraction Study of P2-Na[sub 2/3][Ni[sub 1/3]Mn[sub 2/3]]O[sub 2]," *Journal of The Electrochemical Society* **2001**, *148*, A1225. http://dx.doi.org/10.1149/1.1407247

(11) U. Maitra, R. A. House, J. W. Somerville, N. Tapia-Ruiz, J. G. Lozano, N. Guerrini, R. Hao, K. Luo, L. Jin, M. A. Pérez-Osorio, F. Massel, D. M. Pickup, S. Ramos, X. Lu, D. E. McNally, A. V. Chadwick, F. Giustino, T. Schmitt, L. C. Duda, M. R. Roberts, and P. G. Bruce "Oxygen redox chemistry without excess alkali-metal ions in Na2/3[Mg0.28Mn0.72]O2," *Nature Chemistry* **2018**, *10*, 288-295. http://dx.doi.org/10.1038/nchem.2923

(12) N. Yabuuchi, M. Kajiyama, J. Iwatate, H. Nishikawa, S. Hitomi, R. Okuyama, R. Usui, Y. Yamada, and S. Komaba "P2-type Na-x[Fe1/2Mn1/2]O-2 made from earth-abundant elements for rechargeable Na batteries," *Nat Mater* **2012**, *11*, 512-517. http://dx.doi.org/10.1038/NMAT3309

(13) R. Shanmugam and W. Lai "Na2/3Ni1/3Ti2/3O2: "Bi-Functional" Electrode Materials for Na-Ion Batteries," *ECS Electrochemistry Letters* **2014**, *3*, A23-A25. http://dx.doi.org/10.1149/2.007404eel

(14) L. Zhang, S. X. Dou, H. K. Liu, Y. Huang, and X. Hu "Symmetric Electrodes for Electrochemical Energy-Storage Devices," *Adv. Sci.* **2016**, *3*, 1600115. http://dx.doi.org/10.1002/advs.201600115

(15) Y. Noguchi, E. Kobayashi, L. S. Plashnitsa, S. Okada, and J.-i. Yamaki "Fabrication and performances of all solid-state symmetric sodium battery based on NASICON-related compounds," *Electrochimica Acta* **2013**, *101*, 59-65. http://dx.doi.org/10.1016/j.electacta.2012.11.038

(16) C. Delmas, C. Fouassier, and P. Hagenmuller "Structural Classification and Properties of the Layered Oxides," *Physica B & C* **1980**, *99*, 81-85. http://dx.doi.org/10.1016/0378-4363(80)90214-4

(17) Q. Chen and W. Lai "A Computational Study on P2-Type Nax[Ni1/3Ti2/3]O2as Bi-Functional Electrode Material for Na-Ion Batteries," *Journal of The Electrochemical Society* **2018**, *165*, A3586-A3594. http://dx.doi.org/10.1149/2.1281814jes

(18) Y. F. Mo, S. P. Ong, and G. Ceder "Insights into Diffusion Mechanisms in P2 Layered Oxide Materials by First-Principles Calculations," *Chemistry of Materials* **2014**, *26*, 5208-5214. http://dx.doi.org/10.1021/cm501563f

(19) R. Shanmugam and W. Lai "Study of Transport Properties and Interfacial Kinetics of Na2/3 [Ni1/3MnxTi2/3-x] O2 (x= 0, 1/3) as Electrodes for Na-Ion Batteries," *Journal of The Electrochemical Society* **2015**, *162*, A8-A14. http://dx.doi.org/10.1149/2.0201501jes

(20) Y. J. Shin, M. H. Park, J. H. Kwak, H. Namgoong, and O. H. Han "Ionic conduction properties of layer-type oxides (NaxMx/2Ti1-x/2O2)-Ti-II-O-IV (M=Ni, Co; 0.60 <= x <= 1.0)," *Solid State Ionics* **2002**, *150*, 363-372. http://dx.doi.org/10.1016/S0167-2738(02)00451-4

(21) O. A. Smirnova, R. O. Fuentes, F. Figueiredo, V. V. Kharton, and F. M. B. Marques "Stability and thermal expansion of Na+-conducting ceramics," *J Electroceram* **2003**, *11*, 179-189. http://dx.doi.org/10.1023/B:Jecr.0000026373.56703.B0

(22) R. Hempelmann *Quasielastic neutron scattering and solid state diffusion*; Oxford University Press: Oxford, 2000.

(23) E. Mamontov and K. W. Herwig "A time-of-flight backscattering spectrometer at the Spallation Neutron Source, BASIS," *Rev Sci Instrum* **2011**, *82*. http://dx.doi.org/10.1063/1.3626214

(24) O. Arnold, J. C. Bilheux, J. M. Borreguero, A. Buts, S. I. Campbell, L. Chapon, M. Doucet, N. Draper, R. Ferraz Leal, M. A. Gigg, V. E. Lynch, A. Markvardsen, D. J. Mikkelson, R. L. Mikkelson, R. Miller, K. Palmen, P. Parker, G. Passos, T. G. Perring, P. F. Peterson, S. Ren, M. A. Reuter, A. T. Savici, J. W. Taylor, R. J. Taylor, R. Tolchenov, W. Zhou, and J. Zikovsky "Mantid-Data analysis and visualization package for neutron scattering and mu SR experiments," *Nucl Instrum Meth A* **2014**, *764*, 156-166. http://dx.doi.org/10.1016/j.nima.2014.07.029

(25) R. T. Azuah, L. R. Kneller, Y. M. Qiu, P. L. W. Tregenna-Piggott, C. M. Brown, J. R. D. Copley, and R. M. Dimeo "DAVE: A Comprehensive Software Suite for the Reduction, Visualization, and Analysis of Low Energy Neutron Spectroscopic Data," *J Res Natl Inst Stand Technol* **2009**, *114*, 341-358. http://dx.doi.org/10.6028/jres.114.025

(26) K. S. Singwi and A. Sjölander "Diffusive Motions in Water and Cold Neutron Scattering," *Physical Review* **1960**, *119*, 863-871. http://dx.doi.org/10.1103/PhysRev.119.863

(27) G. Kresse and J. Furthmuller "Efficient iterative schemes for ab initio total-energy calculations using a plane-wave basis set," *Physical Review B* **1996**, *54*, 11169-11186. http://dx.doi.org/10.1103/PhysRevB.54.11169

(28) P. E. Blochl "Projector Augmented-Wave Method," *Physical Review B* **1994**, *50*, 17953-17979. http://dx.doi.org/10.1103/PhysRevB.50.17953

(29) S. Grimme, S. Ehrlich, and L. Goerigk "Effect of the Damping Function in Dispersion Corrected Density Functional Theory," *J Comput Chem* **2011**, *32*, 1456-1465. http://dx.doi.org/10.1002/jcc.21759

(30) S. Grimme, J. Antony, S. Ehrlich, and H. Krieg "A consistent and accurate ab initio parametrization of density functional dispersion correction (DFT-D) for the 94 elements H-Pu," *J Chem Phys* **2010**, *132*, 154104. http://dx.doi.org/10.1063/1.3382344

(31) S. L. Dudarev, G. A. Botton, S. Y. Savrasov, C. J. Humphreys, and A. P. Sutton "Electron-energy-loss spectra and the structural stability of nickel oxide: An LSDA+U study," *Physical Review B* **1998**, *57*, 1505-1509. http://dx.doi.org/10.1103/PhysRevB.57.1505

(32) T. J. Willis, D. G. Porter, D. J. Voneshen, S. Uthayakumar, F. Demmel, M. J. Gutmann, M. Roger, K. Refson, and J. P. Goff "Diffusion mechanism in the sodium-ion battery material sodium cobaltate," *Sci Rep* **2018**, *8*, 3210. http://dx.doi.org/10.1038/s41598-018-21354-5

(33) P. F. Wang, H. R. Yao, X. Y. Liu, Y. X. Yin, J. N. Zhang, Y. R. Wen, X. Q. Yu, L. Gu, and Y. G. Guo "Na+/vacancy disordering promises high-rate Na-ion batteries," *Sci Adv* **2018**, *4*. http://dx.doi.org/10.1126/sciadv.aar6018

(34) D. H. Lee, J. Xu, and Y. S. Meng "An advanced cathode for Na-ion batteries with high rate and excellent structural stability," *Physical Chemistry Chemical Physics* **2013**, *15*, 3304-3312. http://dx.doi.org/10.1039/C2CP44467D

(35) Y. S. Wang, R. J. Xiao, Y. S. Hu, M. Avdeev, and L. Q. Chen "P2-Na-0.6[Cr0.6Ti0.4]O-2 cation-disordered electrode for high-rate symmetric rechargeable sodium-ion batteries," *Nat Commun* **2015**, *6*. http://dx.doi.org/10.1038/Ncomms7954

(36) C. Zhao, Z. Yao, Q. Wang, H. Li, J. Wang, M. Liu, S. Ganapathy, Y. Lu, J. Cabana, B. Li, X. Bai, A. Aspuru-Guzik, M. Wagemaker, L. Chen, and Y.-S. Hu "Revealing High Na-Content P2-Type Layered Oxides as Advanced Sodium-Ion Cathodes," *J Am Chem Soc* **2020**, *142*, 5742-5750. http://dx.doi.org/10.1021/jacs.9b13572

(37) N. Bucher, S. Hartung, J. B. Franklin, A. M. Wise, L. Y. Lim, H.-Y. Chen, J. N. Weker, M. F. Toney, and M. Srinivasan "P2–NaxCoyMn1–yO2 (y = 0, 0.1) as Cathode Materials in Sodium-Ion Batteries—Effects of Doping and Morphology To Enhance Cycling Stability," *Chemistry of Materials* **2016**, *28*, 2041-2051. http://dx.doi.org/10.1021/acs.chemmater.5b04557